Comparing Turbulence Models for CFD Simulation of UAV Flight in a Wind Tunnel Experiments

Saif Aljuhaishi[1*], Yaseen K. Al-Timimi[1], Basim I. Wahab[1]

[1] Department of Atmospheric Sciences, College of Science, Mustansiriyah University, Palestine Street, P.O.B. 14022, 10011 Baghdad, IRAQ
[*] Corresponding author, e-mail: saifaljuhaishi@uomustansiriyah.edu.iq

Abstract

Wind tunnel tests are costly and time-consuming, and the accuracy of the tests is limited by the size of the tunnel, to solve this problem, researchers use computational fluid dynamics (CFD) to conduct wind tunnel experiments using a computer because it is less timely and less costly. Computerized testing of drone's models using wind tunnel experiment simulation in computational fluid dynamic (CFD) software requires knowledge of the most suitable turbulence model for this drone. In this paper ANSYS fluent program has been used to test four most common turbulence models for use (Spalart-Allmaras, K-Epsilon, K-Omega and Reynolds stress) and laminar flow on the ScanEagle drone model (an aerial reconnaissance drone used in military and intelligence operations) and calculated their effect on aerodynamic parameters In terms of accuracy and time to solution, concluded that the best turbulence model in terms of balancing accuracy and the time taken for the calculation is K-Omega model.

Keywords

K-Omega, aircraft, K-Epsilon, drone, ScanEagle, ANSYS, Spalart-Allmaras

1 Introduction

Unmanned Aerial Vehicles (UAVs) have gained significant traction in scientific research because of their versatility in areas like military applications, surveillance, photography, and agriculture. As a result of lower operational and manufacturing costs when compared to manned vehicles. They can be used for a variety of tasks, such as road traffic, search and rescue operations, border patrol missions, and fire monitoring. UAVs are typically chosen for missions that require a lot of pilot effort and that are deemed hazardous (Costache et al., 2022). Most engineering flows exhibit turbulent characteristics when working with CFD simulations, and these flows require solution. As one of the most important aspects of CFD modeling, proper turbulence modeling can produce consistent and useful CFD outputs (Somashekar and Immanuel, 2021).

As the aircraft is taking shape, the need for a more thorough aerodynamic analysis has arisen in order to verify the assumptions made, and to see if there are any aerodynamically bad areas that need to be addressed closer. The creation of a scale model and wind tunnel tests are very costly, therefore a more theoretical approach using CFD makes sense in order to make progress with the project. In literature, several aerodynamic studies are available. Zia Ur Rehman study, time-domain analytical method for aeroelastic analysis of high aspect ratio wing using unsteady indicial aerodynamics (Rehman, 2022). Mouton et al. (Mouton et al., 2012) study, combined wind tunnel tests and flow simulations for light aircraft performance prediction, they provide an example of how to derive all of the aerodynamic properties of a lightweight, low-speed aircraft design using the ONERA L2 wind tunnel in conjunction with CFD computations. El Bahlouli et al. (El Bahlouli et al., 2019), study, they conclude the model can replicate features of the atmospheric boundary layer, including the coriolis force and shallow boundary layer, according to a validation study based on the leipzig experiment. Karkoulias, et al. (Karkoulias, et al., (2022), looked into single and multiphase flow over the surface of a specially-designed wing with an Eppler-420 airfoil and an independent custom-designed blended winglet, simulating the flow of air and solid particles over a wildfire. They found that the structured mesh was found to be more realistic than the unstructured and mosaic meshes, with a good agreement between simulations and experiments.

Lastly, because of the solid particles, a decrease in the wing section's aerodynamic efficiency is seen. Liu et al. (Liu et al., 2023), compared the aerodynamic parameters while altering the freestream velocity, to look into the benefits and drawbacks of using the three distinct approaches. Considering its limitations, the BEMT proves to be a dependable method for estimating the aerodynamic parameters of a fixed-pitch propeller on a small scale. Thai, et al. (Thai, et al., 2022), used the high-fidelity rotorcraft simulation framework HPCMP CREATE-AV helios to investigate the effects of turbulence modeling techniques on the prediction of a small quadrotor unmanned aerial vehicle. Predicting the aerodynamic performance of small-scale rotorcraft is demonstrated to be a good fit for the helios simulation suite. Adanta et al. (Adanta et al., 2020), study, comparison of standard K-epsilon and SST K-omega turbulence model for breastshot waterwheel simulation, they deduced that the SST K-omega model and the standard K-epsilon model produced results that were comparable. As a result, the standard K-epsilon model will yield a more efficient simulation for the breastshot waterwheel than the SST K-omega model due to its lower computational requirements. Nonetheless, the SST K-omega model is recommended for research on physical phenomena. (Menter, 1993) study zonal two equation k-w turbulence models for aerodynamic flows, the results showed that while the SST model's predictions are independent of free strearn values, they more closely match experimental findings for adverse pressure gradient boundary-layer flows.

Two ideas that are frequently misapplied and lead to confusion are endurance and range. Although endurance is the longest period of time, Range is the furthest an aircraft can fly under specific flight conditions before needing to refuel (Gunston, 2013). The breguet equations, which are frequently found in the imperial unit system, can be used to mathematically define these ideas. These demonstrate that for propeller-driven aircraft, endurance depends on $C_L^{3/2}/C_D$ and range depends on L/D ratio. Lift and drag are the two factors that determine performance coefficients, so optimizing them can be achieved by either raising lift or lowering drag (Roskam et al., 1997).

This paper uses the range (described by the lift and drag coefficients) to describe the effect of selecting the appropriate turbulence model on the aerodynamic performance under standardized boundary conditions, four different turbulence models and laminar flow were tested for ScanEagle UAVs by CFD.

2 Initial configuration

The ScanEagle drone used in this paper, and its characteristics are shown in Table 1, was produced by Boeing company and used in the US navy and some countries in the middle east. Fig. 1 shows the engineering of the UAV.

ANSYS 2019 (ANSYS, 2019) programs were used to modify and process the drone design (ANSYS, 2019), to create domains (SpaceClaim and DesignModeler), to generate the mesh (ANSYS mesher), to prepare and implement the simulation process (fluent) and to present the results (CFD Post).

The given engineering design cannot be used directly in a ANSYS programs, since programs of this type require more detail than computer aided design AutoCAD programs (Autodesk, 2020). Therefore, before importing in ANSYS fluent 2019, it was necessary to design the geometry in AutoCAD software and perform further operations in SpaceClaim and DesignModeler as shown in Table 2.

Analysis and simulation of drone flight was performed using a computer with AMD Ryzen 7 4800 H processor and RAM = 32 GB to run ANSYS fluent 2019 applications on steady state, absolute velocity, and incompressible (pressure dependent) stream. The simplification of the incompressible flow is very reasonable, since the compression effects of the Mach number (0.11655) are low, it is small enough to be neglected at mach numbers below (0.3). Flow is assumed to be adiabatic, which means there is no heat exchange between

Table 1 UAV characteristics (ScanEagle, 2023)

Feature	value
Wingspan	3.1 meters
Length	1.6 meters
Weights	22 kilograms
Speed	25–30 m/s (cruise) 40 m/s (max)
Endurance	12+ hours
Altitude	5,000+ meters
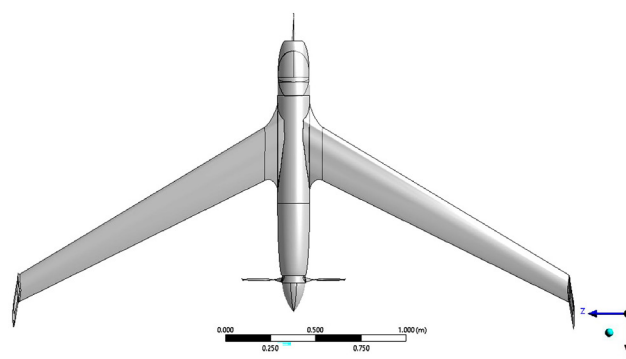
Fig. 1 ScanEagle Drone geometry

Table 2 UAV geometry modification results

Properties	Before editing	After editing
Parts (bodies)	131	1
Faces	396	66
Edges	1185	171
Vertices	924	112

the drone and the surrounding atmosphere. The acceleration of gravity towards Earth is (9.8) m/s².

The best practice guidelines, provided by (Xu, et al., 2023), were followed, 3D two dominoes have been created around the drone model to represent the area in which the wind tunnel (it is a specifically created, protected area into which air is drawn, or blown, mechanically to a predetermined speed and flow pattern at a specific moment) (Roomi, 2016) experiment is to be tested Its dimensions are shown in Fig. 2. Both domains were meshed with different characteristics for each, As shown in Table 3 and Fig. 3, the total
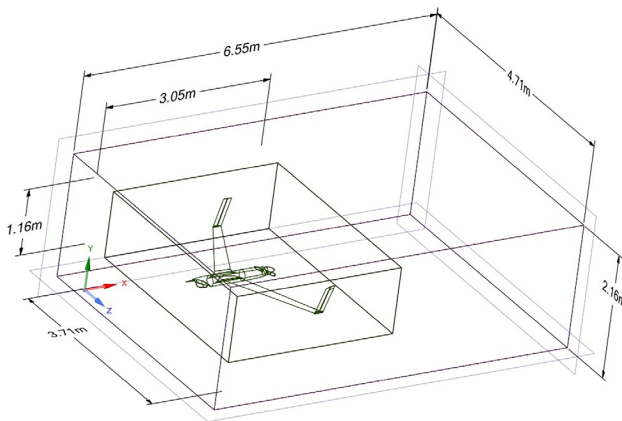
Fig. 2 Wind tunnel domains dimensions

Table 3 UAV geometry modification results

| Object Name	inner domain	outer domain
Volume	13.12598 m³	66.63708 m³
Nodes	2657393	455459
Elements	15397032	426199
Method	Tetrahedrons	Hex Dominant
Element Size	2.e-002 m	5.e-002 m
Smoothing		High
Mesh Metric Aspect Ratio (average)	1.77991684617529	1.02831163963311
Mesh Metric Element Quality (average)	0.85441494273655	0.996875710854774
Mesh Metric Skewness (average)	0.201882003783055	0.0121648908201659
Orthogonal Quality (average)	0.797015510917134	0.997817037476354
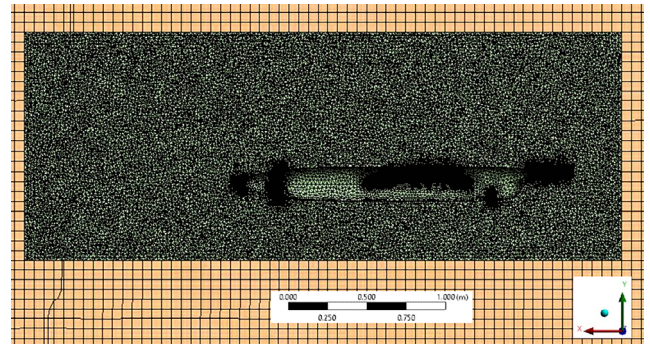
Fig. 3 The Mesh method and shape

number of elements was 15,823,231, and the total number of nodes was 3,112,852.

3 Boundary conditions

The boundary condition at the inlet was set to a velocity of 30 m/s normal to the inlet in order to simulate the freestream. As a result, the flow would be parallel to the longitudinal *x*-axis of the model. The reference pressure used by ANSYS fluent was set to 101325 pa for the total pressure at the outlet boundary. Consequently, there will be no resistance or draw out for the air leaving the control volume, allowing it to exit at a velocity higher than usual.

4 Solution method

The coupled method was used to solve the Reynolds-averaged Navier–Stokes equations (RANS), continuity equation, and energy equation, which represent conservation of momentum (product between a particle's mass and velocity (kg × m/s) (Mehson and Hassoon, 2019), conservation of mass, and conservation of energy (the energy of interacting objects or molecules in a closed system remains constant) (Fattah and et al., 2021), respectively. As well as to solve the three-dimensional equations of turbulent kinetic energy (It is particularly significant in microfluid dynamics since it has a direct bearing on momentum transfer via the boundary layer (Mohammed, 2016) and turbulent dissipation (Thomson, 1971).

In the aforementioned equations and the turbulence model equations, residual monitors were 10^{-6}. The solution will keep solving until it reaches convergence or finishes 100 iterations.

5 Spalart-Allmaras (SA) model

Developed primarily for aerodynamic flows, a one-equation turbulence model is the Spalart-Allmaras model. This model represents an equation of transport for eddy viscosity. Finding the Reynolds stress distribution would be the first

step towards creating a closed system representation of the flow's mean motion using the central equation.

Any transportable scalar quantity, like eddy viscosity, is typically transported using the following equation, subject to the conversion laws, is transported according to the following equation (Kostic, 2015):

$$\frac{DF}{Dt} = \frac{\partial F}{\partial t} + (u.\nabla)F = \text{Diffusion} + \text{Production} - \text{Destruction}$$

(1)

It is necessary to precisely define each diffusion, production, and destruction term in order to build a complete model for a turbulent flow. The process of defining and non-dimensionalizing these terms will result in some additional constants and non-dimensional functions in each term.

A transport formula for the working variable $\tilde{v}$ of (intermediate) turbulence is written as (Spalart and Allmaras, 1992):

$$\frac{\partial \tilde{v}}{\partial t} + u_j \frac{\partial \tilde{v}}{\partial x_j} - \frac{\partial}{\partial x_j}\left[\frac{(v+\tilde{v})}{\sigma}\frac{\partial \tilde{v}}{\partial x_j}\right] = c_{b1}\tilde{\omega}\tilde{v} - c_{\omega 1}f_\omega\left(\frac{\tilde{v}}{d}\right)^2$$
$$+\frac{c_{b2}}{\sigma}\frac{\partial \tilde{v}}{\partial x_i}\frac{\partial \tilde{v}}{\partial x_i}$$

(2)

Where $\tilde{\omega}$: modified vorticity, d: the separation between walls, the model utilized here has the closure constants $cb_1 = 0.1355$, $cb_2 = 0.622$, $cw_1 = 3.2391$, and $\sigma = 2/3$.

6 K-Epsilon (k-ε) model
The k-ε models' transport equations rely on the dissipation rate, ε, and the turbulent kinetic energy, k. Launder and Spalding's standard k-ε model is predicated on the idea that flow is completely turbulent. Better results are obtained with this model for fully turbulent flows. The following are the transport equations for the typical k-ε model. (Noorbakhsh et al, 2019):

For k:

$$\frac{\partial}{\partial t}(pk) + \frac{\partial}{\partial x_i}(pkv_j) = \frac{\partial}{\partial t}\left[\left(\mu + \frac{\mu}{\sigma_k}\right)\frac{\partial k}{\partial t}\right] + G_k + G_b$$
$$+\rho \in -Y_M + S_k$$

(3)

And for ϵ:

$$\frac{\partial}{\partial t}(\rho \in) + \frac{\partial}{\partial t}(\rho \in v_j) = \frac{\partial}{\partial t}\left[\left(\mu + \frac{\mu_t}{\sigma_\in}\right)\frac{\partial \in}{\partial t}\right]$$
$$+\rho C_1 + \rho C_2 \frac{\in^2}{k + \sqrt{v \in}} + C_1 \frac{\in}{k}C_{3\in}C_b + S_\in$$

(4)

Where G_b is generation of turbulence kinetic energy (TKE) due to buoyancy, G_k is generation of TKE due to the mean velocity gradients, μ is the viscosity, μ_t is the turbulent viscosity, S_ε and S_k and S_e are user defined source terms. $C_1 = 1.44$, $C_2 = 1.92$.

7 SST K-Omega (k-ω) model
The SST k-ω turbulence model is a common two-equation eddy-viscosity model. Because the SST k-ω model uses a k-ω formulation in the inner regions of the boundary layer, it is directly applicable all the way down to the wall through the viscous sub-layer, allowing it to be used as a low-re turbulence model without the need for additional damping functions (Spalart and Allmaras, 1992). Additionally, by adopting a k-ε behavior in the free-stream, the SST formulation circumvents the prevalent k-ω problem, which arises from the model's excessive sensitivity to the inlet free-stream turbulence properties. The two k-w model equations can be written as (Adanta et al, 2020):

For k:

$$\frac{\partial}{\partial t}(\rho k) + \frac{\partial}{\partial x_i}(\rho k u_i) = \frac{\partial}{\partial x_i}\left[\Gamma_k \frac{\partial k}{\partial x_j}\right] + G_k - Y_k + S_k$$

(5)

And for ω:

$$\frac{\partial}{\partial}(\rho\omega) + \frac{\partial}{\partial x_i}(\rho\omega u_i) = \frac{\partial}{\partial x_i}\left[\Gamma_\omega \frac{\partial \omega}{\partial x_j}\right] + G_\omega - Y_\omega + D_\omega + S_\omega$$

(6)

Where G_ω and G_k are the generation of ω and k respectively, Γ_ω and Γ_k are the effective diffusivity of ω and k respectively. Y_ω and Y_k are the dissipation of ω and k in the turbulence respectively, D_ω is the cross diffusion, S_ω and S_k are the source terms.

8 Reynolds-stress transport model
The precise formula governing the Reynolds-stress transport for incompressible flows can be written as: (Noorbakhsh et al., 2019)

$$\frac{D}{Dt}\overline{u_i u_j} = -\left(\overline{u_j u_k}\frac{\partial U_i}{\partial x_k} + \overline{u_i u_k}\frac{\partial U_j}{\partial x_k}\right) - 2v\frac{\partial u_i}{\partial x_k}\frac{\partial u_j}{\partial x_k} + \frac{1}{\rho}p$$
$$\left(\frac{\partial u_i}{\partial x_j} + \frac{\partial u_j}{\partial x_i}\right) - \frac{\partial}{\partial x_k}\left\{\overline{u_i u_j u_k} - v\frac{\partial}{\partial x_k}\overline{u_j u_k} + \frac{1}{\rho}\overline{p(u_j\delta_{ik} + u_i\delta_{jk})}\right\}$$

(7)

where the summation convention is applied for repeated suffices and overbars indicate the ensemble averaging.

The equation's terms on the right side are generation, dissipation, redistribution, and diffusion.

9 Results and discussions

According to Bernoulli's principle of fluid dynamics, a fluid's speed increases when its static pressure or fluid pressure decreases. Bernoulli deduced that pressure decreases when the flow speed increases (Marciotto, 2016). As a result of the design of the wing, the upper part of the wing is curved and the lower part is flat, meaning that the air at the top of the wing travels a greater distance to reach the end of the wing compared to the lower part and in the same period of time, and this means the wind speed at the top of the wing is greater than at the bottom, and therefore the pressure at the top of the wing is low at the top of the wing and high at the bottom, and this situation is clear in Figs. 4, 5, 6.

Figs. 4, 5, 6 illustrate a scaneagle drone cruise, at flow velocity (30 m/s), angle of attack (0) and boundary conditions for standard atmosphere at sea level, pressure (101325) pa, density (1.225 kg/m³), temperature (298 k), and viscosity (1.7894×10–05 kg/m²). Fig. 4 represents the flow pressure at the top of the plane for (A) laminar flow and the four turbulence models (B) Spalart-Allmaras (SA) model, (C) K-Epsilon (KE) model, (D) K-Omega (KW) model and Reynolds stress (RS) model.

Figs. 4, 5 explain that the pressure at the front of the drone is higher than the rest of the parts, because the front of the drone is in direct friction with the air flow (wind) surrounding the plane, and a pressure gradient occurs above and below the wing due to the formation of small vortices as a result of the turbulence to be the lowest pressure is in the center of the wing, then the pressure increases to reach the end of the wing. We also notice that there is a pressure gradient that starts with high pressure from the far end of the wing towards the body of the drone, due to the presence of vertical ailerons at the ends of the wings of the drone. As illustrated in Fig. 7, we also observed that the pressure values across the models vary due to the different mathematical approaches taken by each turbulence model. The Reynolds stress model is the most accurate since it solves (7) turbulence equations, which causes small vortices to appear in it. These small vortices are combined and approximated by the remaining models. It is not assumed that there is a turbulence model in the case of laminar flow.

Fig. 6 shows that the method of solving the K-omega model is the closest to the method of solving the Reynolds stress model because the results are very close compared to the rest of the models.
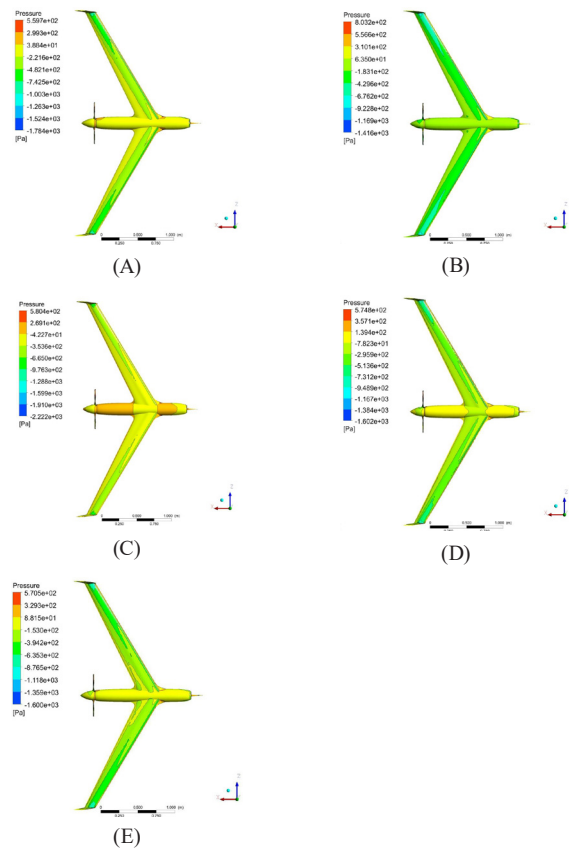

Fig. 4 Pressure at the top of the drone, (A) laminar flow, (B) SA model, (C) KE model, (D) KW model and (E) RS model
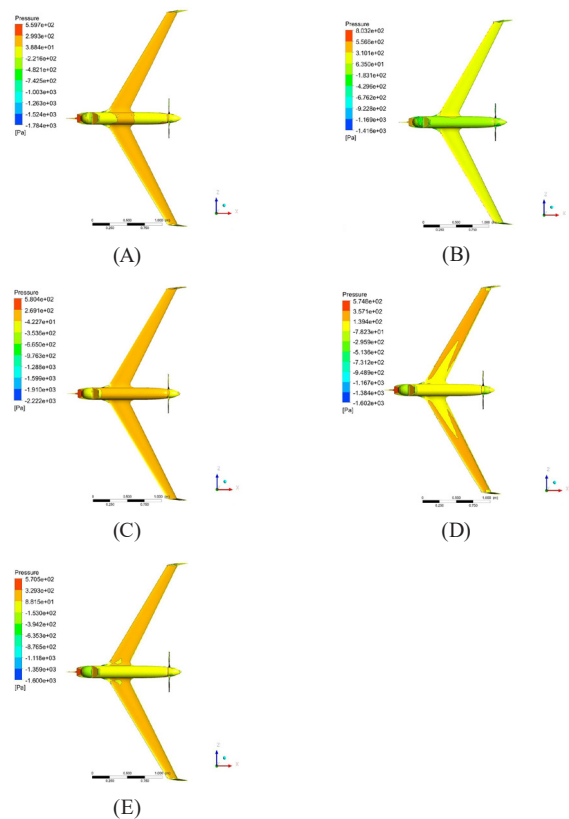

Fig. 5 Pressure at the bottom of the drone, (A) laminar flow, (B) SA model, (C) KE model (D KW model and (E) RS model
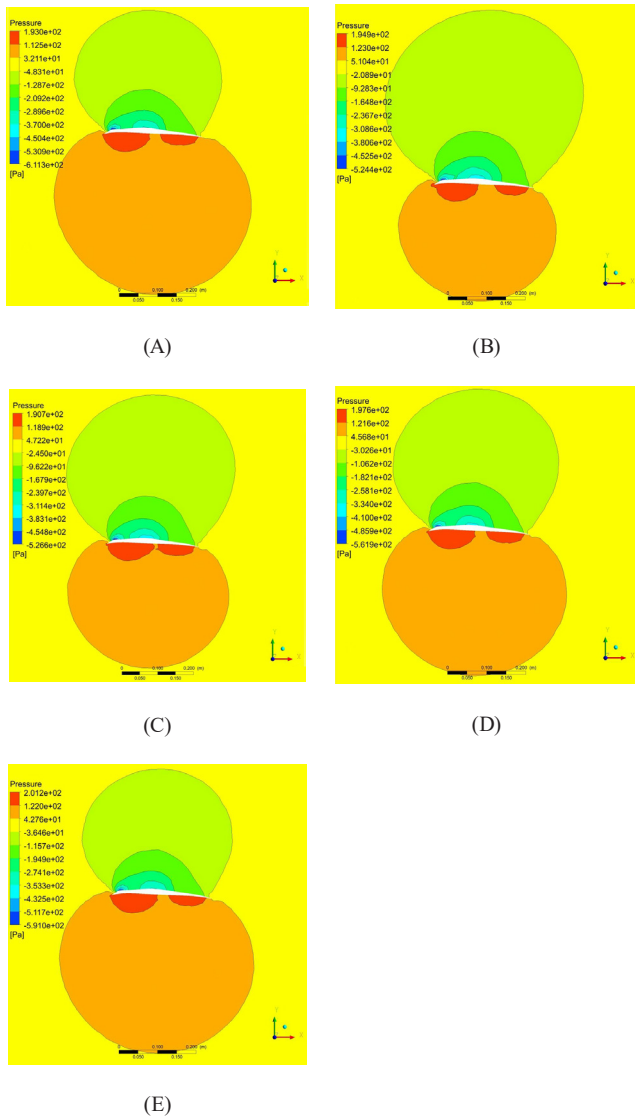
(A)

(B)

(C)

(D)

(E)

Fig. 6 Pressure around the wing of the drone, (A) laminar flow, (B) SA model, (C) KE model, (D) KW model and (E) RS model
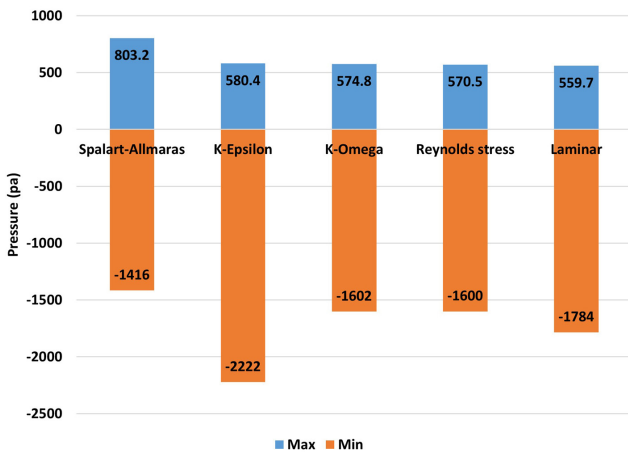

Fig. 7 The maximum and minimum value of pressure for drone in Figures 4, 5

Fig. 6, shows that the pressure at the bottom of the wing is greater than at the top of the wing, the pressure at the front of the wing is higher than the rest of the parts, a pressure drop occurs the top and bottom of the wing as a result of the formation of small vortices due to turbulence, so that the lowest pressure is in the center of the wing, then the pressure increases to reach the end of the wing.

Fig. 8 shows the maximum and minimum value of pressure for the wing of the UAV shown in Fig. 6. We note that the results of the K-omega model solution are closest to the results of the Reynolds stress model solution compared to the solutions of other turbulence models.

Fig. 9 shows the change in the lift coefficient (C_l) with the change in the Reynolds number (Re) affected by the change in flow velocity, which was solved using the four turbulence models and laminar flow model. There is a difference in the value of C_l with the difference in the turbulence model used for the solution, and this difference increases with increasing Re and speed, and the difference decreases with decreasing Re and speed. the results note that C_l is the highest in laminar flow because he neglects in his calculations the occurrence of disturbance around the wing that hinders the lifting force, and that C_l increases as the number of equations increases The turbulence used
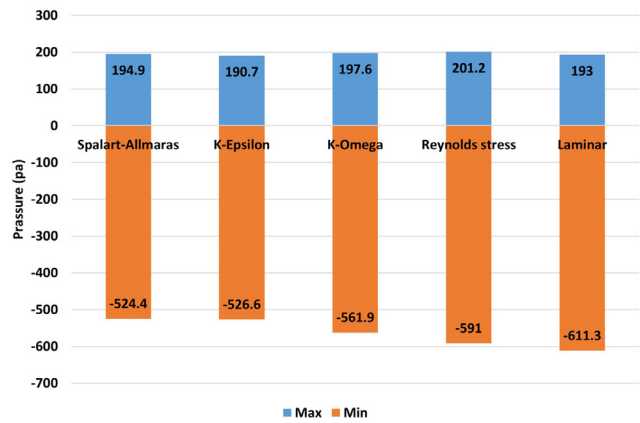

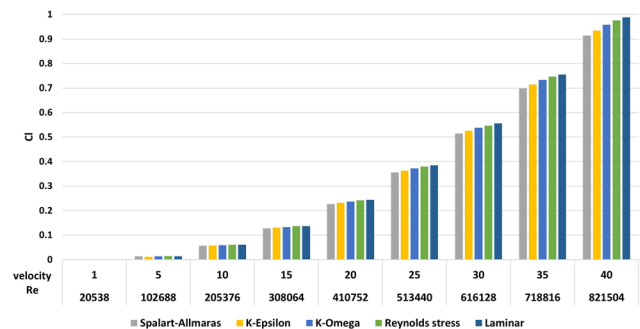**Fig. 8** The maximum and minimum value of pressure for drone's wing from results shows in Fig. 6

Fig. 9 Change in C_l with Re affected by flow velocity, for turbulence models and laminar flow

by the model due to an increase in the number and size of vortices calculated by the model. The results notice that the value of C_l calculated by the K-omega model is closer to its value calculated by the more accurate Reynolds model, therefore it is better than the other two models, and the K-epsilon model is better than the Spalart-Allmaras model.

Fig. 10 shows the change in the value of the drag coefficient (C_d) with the change in the value of the Reynolds number (Re) affected by the change in the flow velocity. the results notice an increase in the value of C_d with the increase in Re, and there is a difference in the value of C_d with the difference in the turbulence model used for the solution, this difference increases as Re and speed increase. C_d is the lowest in laminar flow due to an increase in the number and size of vortices calculated by the model that hinders the movement of the aircraft, and that C_d decreases as the number of turbulence equations used by the model increases due to the increase in area covered by the high pressure at the front of the drone, we notice that the C_d value calculated by the K-omega model is the closest to its value calculated by the most accurate Reynolds stress and therefore it is better than the other two models, just as the K-epsilon model is better than the Spalart-Allmaras model.

Fig. 11 shows the change in range represented by the ratio C_l/C_d with the change in the Reynolds number (Re) affected by the change in flow velocity. There is a difference in the value of C_l/C_d with the difference in the turbulence model used for the solution, and this difference increases with increasing Re and speed, and the difference decreases with decreasing Re and speed, and we note that C_l/C_d is the highest in laminar flow due to an increase in the number and size of vortices calculated by the model that hinders the lifting force, and that C_l/C_d increases whenever the number of turbulence equations used by the model increases due to the decrease in the maximum pressure calculated by the turbulence model which is at the front of the wing.
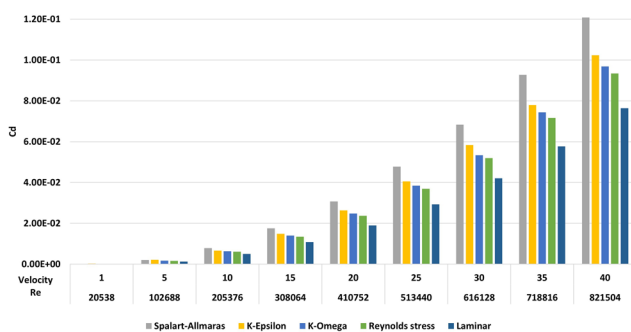
Characteristics of the Reynolds stress model unlike the models discussed earlier, it solve the Reynolds stresses directly and offer comprehensive details regarding the anisotropic nature of the turbulence. Because of this, it is typically applied to extremely complicated turbulent flows with significant anisotropic effects. However, it demands fine mesh resolution, is computationally costly, frequently needs a large amount of validation data, and takes longer to solve. K-omega model more accurate forecasts for separated flows, and better handling of near-wall flows than the k-ϵ model make it suitable for complex flows with large adverse pressure gradients. For flows with significant streamline curvature, rotation, or intricate near-wall turbulence, the k-ϵ model's accuracy is limited. The Spalart-Allmaras model uses a single transport equation for the eddy viscosity to directly solve for the turbulent viscosity. It is computationally efficient, and easy to implement. However, it loses accuracy for intricate flows that include a lot of rotation or streamline curvature.

The results note that the value of C_l/C_d calculated according to the K-omega model is closer to its value calculated by the more accurate Reynolds stress model, and therefore it is Better than the other two models, and the K-epsilon model is better than the Spalart-Allmaras model.

The duration has an impact on how long it takes to test new and modified airplane models. As such, it is imperative to select a disturbance model with high or acceptable accuracy for the solution and one that solves the problem quickly. The time period for the solution with the changed turbulence models is displayed in Fig. 12. The number of turbulence equations used for each model increases, we observe an increase in the solution's time period. Because there are no turbulence equations for the laminar flow to solve, it takes less time. Therefore, for the models Spalart-Allmaras, K-epsilon, K-omega, and Reynolds stress, respectively, the solution period increases.
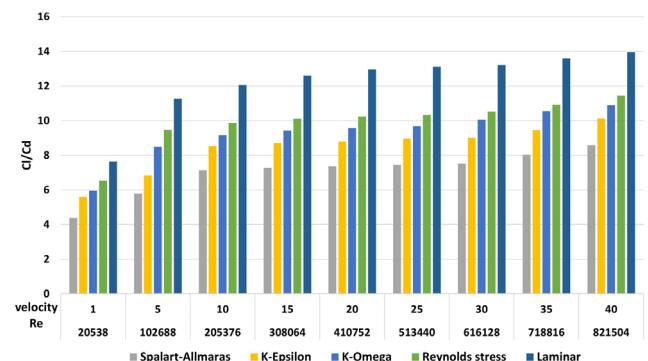

Fig. 10 Change in Cd with Re affected by flow velocity, for turbulence models and laminar flow

Fig. 11 Change in Cl/Cd ratio with Re affected by flow velocity, for turbulence models and laminar flow
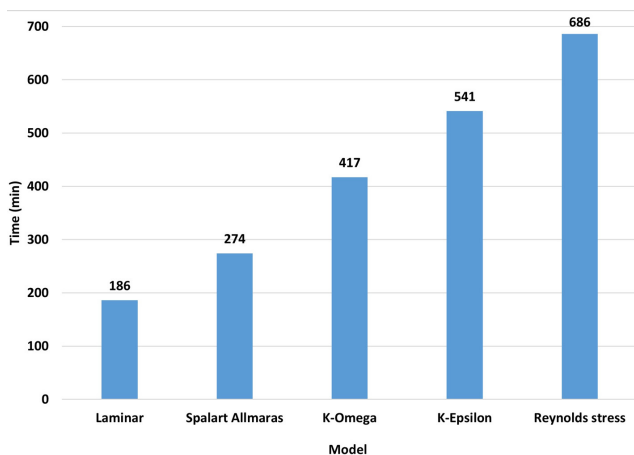
Fig. 12 Time period for the solution with the change in the turbulence models

10 Conclusions

The following summarizes the main conclusions of this work: In terms of accuracy of results, aerodynamic coefficients (Lift and drag) changed significantly among turbulence models, with laminar flow showing the highest lift coefficient and the lowest value for the drag coefficient due to neglecting disturbances. The K-omega model closely matched the Reynolds stress model in predicting aerodynamic coefficients and pressure distribution. K-epsilon and Spalart-Allmaras models showed discrepancies compared to the more accurate Reynolds stress and K-omega models, with the former generally outperforming the latter.

In terms of Computational Efficiency, The solutions time increased with the complexity of turbulence models. Laminar flow simulations were the fastest, while Reynolds stress model simulations took the longest due to solving multiple turbulence equations. The solution using the K-omega model were faster than using K-epsilon and Reynolds stress models, but it was slower than the Spalart-Allmaras model and laminar flow.

Finally, we conclude that the K-omega model is the best model for simulating drone flight using CFD if it is important to reconcile the high accuracy of the results with a shorter solution time, especially for drones with complex models. The Reynolds stress model is chosen if accuracy is more important at the expense of the time taken for the solution. The Spalart-Allmaras model can be used to simulate drone flight with simple (Primary) models if faster solution is important but with reasonable accuracy.

References

Adanta, D., Muhammad, N. M., Fattah, I. M. R. (2020) "Comparison of standard K-ε and SST K-ω turbulence model for breastshot waterwheel simulation", Journal of Mechanical Science and Engineering, 7(2), pp. 039–044.
https://doi.org/10.36706/jmse.v7i2.44

Ansys "Ansys, (2019)" [computer program] Available at: https://www.ansys.com [Accessed: 02 November 2023]

Autodesk "AutoCAD, (2020)", [computer program] Available at: https://www.autodesk.co.uk/products/autocad/overview?term=1-YEAR&tab=subscription [Accessed: 8 November 2023]

Costache, F., Nichifor, S.-E., Costea, M.-L., Ioniță, A. (2022) "Automatic approach procedure of a flying vehicle on a mobile platform using backstepping controller", Incas Bulletin, 14(4), pp. 51–62.
https://doi.org/10.13111/2066-8201.2022.14.4.5

El Bahlouli, A., Rautenberg, A., Schön, M., Berge, K. Z., Benge, J., Knaus, H. (2019) "Comparison of CFD simulation to UAS measurements for wind flows in complex terrain: application to the winsent test site", Energies, 12(10), 1992.
https://doi.org/10.3390/en12101992

Fattah, A., Ahmed, M. M., Abd, N. M. (2021) "The relationship between air stability and visibility over Baghdad city", Al-Mustansiriyah Journal of Science, 32(2), pp. 82–89.
https://doi.org/10.23851/mjs.v32i2.988

Gunston, B. (2013) "The Cambridge aerospace dictionary", Cambridge University Press, ISBN 9780521191654

Karkoulias, D. G. Tzoganis, E. D., Panagiotopoulos, A. G., Acheimastos, S. G. D., Margaris, D. P. (2022) "Computational fluid dynamics study of wing in air flow and air–solid flow using three different meshing techniques and comparison with experimental results in wind tunnel", Computation, 10(3), 34.
https://doi.org/10.3390/computation10030034

Kostic, C. (2015) "Review of the Spalart-Allmaras turbulence model and its modifications to three-dimensional supersonic configurations", Scientific Technical Review, 65(1), pp. 43–49.
https://doi.org/10.5937/str1501043k

Liu, X., Zhao, D., OO, N. L. (2023) "Comparison studies on aerodynamic performances of a rotating propeller for small-size UAVs", Aerospace Science and Technology, 133, 108148.
https://doi.org/10.1016/j.ast.2023.108148

Marciotto, E. R. (2016) "Classic Bernoulli's principle derivation and its working hypotheses", Physics Education, 51(4), 045005.
https://doi.org/10.1088/0031-9120/51/4/045005

Mehson, M. Z., Hassoon, A. F. (2019) "Determination of heat and momentum fluxes over Baghdad city", Al-Mustansiriyah Journal of Science, 30(1), pp. 23–32.
https://doi.org/10.23851/mjs.v30i1.146

Menter, F. (1993) "Zonal two equation k-w turbulence models for aerodynamic flows", [preprint] 23rd Fluid Dynamics, Plasmadynamics, and Lasers Conference, (Day Month Year)
https://doi.org/10.2514/6.1993-2906

Mohammed, N. A. (2016) "The effect of solar radiation on turbulent kinetic energy (TKE) over Baghdad city", Mustansiriyah Journal of Science, 27(1), pp. 11–14.

Mouton, S., Rantet, E., Gouverneur, G., Verbeke, C. (2012) "Combined wind tunnel tests and flow simulations for light aircraft performance prediction", Aerodynamics 2012 (47th AAAF International Symposium of Applied Aerodynamics, Wind tunnel and computation: a joint strategy for flow prediction), Paris, France. [online] Available at: https://hal.science/hal-03017137 [Accessed: Day Month Year]

Noorbakhsh, M., Zaboli, M., Mousavi Ajarostaghi, S. S. (2019) "Numerical evaluation of the effect of using twisted tapes as turbulator with various geometries in both sides of a double-pipe heat exchanger", Journal of Thermal Analysis and Calorimetry, 140(3), pp. 1341–1353.
https://doi.org/10.1007/s10973-019-08509-w

Rehman, Z. U. (2022) "Time-domain analytical method for aeroelastic analysis of high aspect ratio wing using unsteady indicial aerodynamics", Incas Bulletin, 14(3), pp. 85–99.
https://doi.org/10.13111/2066-8201.2022.14.3.8

Roomi, T. O. (2016) "Designing an open circuit wind tunnel for atmospheric boundary layers", Diyala Journal for Pure Sciences, 12(3), pp. 12–25. [online] Available at: https://www.iasj.net/iasj/download/3bffa0a609de6aa2 [Accessed: Day Month Year]

Roskam, J., Tau, C., Lan, E. (1997) "Airplane aerodynamics and performance", DAR corporation, ISBN 978-1-884885-44-0

ScanEagle "INSITU", [online] Available at: https://www.insitu.com/products/scaneagle [Accessed: 27 November 2023]

Somashekar, V., Immanuel S. R. A. (2021) "Comparative study on the prediction of aerodynamic characteristics of Mini – unmanned aerial vehicle with turbulence models", International Journal of Aviation, Aeronautics, and Aerospace 8(1), pp. 1–19.
https://doi.org/10.15394/ijaaa.2021.1559

Spalart P. R, Allmaras S. R. (1992) "A one-equation turbulence model for aerodynamic flows", AIAA, 439(1), pp. 5–21.

Thai, A. D., Grace, S. M., Jain, R. (2022) "Effect of turbulence modeling selection within Helios for small quadrotor aerodynamics", Journal of Aircraft, 59(4), pp. 927–945.
https://doi.org/10.2514/1.c036410

Thomson, W. T. (1971) "Theory of vibrations with applications", Prentice Hall, ISBN 0748743804

Xu, S., Zhao, J., Wu, H., Zhang, S., Müller, J.-D., Huang, H., Rahmati, M., Wang, G. (2023) "A review of solution stabilization techniques for RANS CFD solvers", Aerospace, 10(3), 230.
https://doi.org/10.3390/aerospace10030230